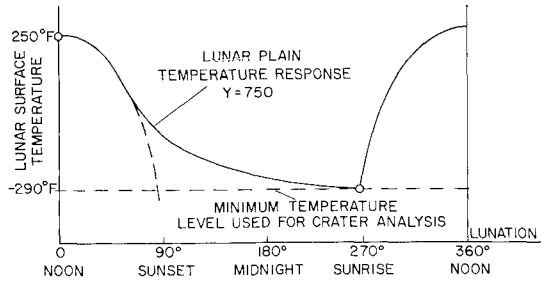

Fig. 5 Temperature response of the lunar surface.

where

$$\zeta \equiv (4/a^2 + 1)q_s + (S \sin\delta)/(a^2/4 + 1) \qquad (23)$$

and $\mathbf{s}\cdot\mathbf{n}$ is the scalar product of the solar ray unit vector $\mathbf{s}$ and crater surface unit normal vector $\mathbf{n}$.

Discussion of Results

The temperature relation for the shadowed region indicates that for the case of $q_s = 0$, the surface temperature of the crater approaches 0°R when $\delta = 0$, i.e., between sunset and sunrise points. This is not in agreement with lunar surface temperature data obtained by experimental methods. In effect, the minimum lunar surface temperature is not lower than ~170°R, because of the thermal inertia of the lunar soil. During the lunar day, the thermal energy penetrates into the soil and at night, it reverses the direction and flows toward the outside. As an approximation, the outward flowing heat can be considered as a surface source in the heat balance equation for lunar night and lunar shadow conditions. Taking T_s = 170°R as the minimum "level," the equivalent surface source is

$$q_s = \sigma T_s^4 = 1.4 \text{ Btu/hr-ft}^2$$

Figure 4 illustrates crater temperature distribution for 3:1 and 8:1 aspect ratio craters at various solar elevations. Shadow temperatures, which are constant, were computed based on the surface source approximation. It can be shown that by carrying on the source q_s in the computation of the crater temperatures in the sunlit region, the error introduced by the approximation is less than 1°R for $\delta = 90°$ and a 3:1 aspect ratio crater.

The black-body equilibrium temperature of the lunar plain at $\delta = 90°$ is approximately 250°F (710°R). In comparison, the maximum temperature in a 3:1 aspect ratio crater is 300°F, in an 8:1 crater, 260°F.

Figure 5 illustrates the surface source approximation to account for the thermal inertia of the lunar soil. The response curve was originally observed by Pettit and Nicholson[1] and later derived analytically by Jaeger.[2] Recent data obtained by Surveyor experiments are in good agreement with earlier findings,[3] with the exception of the numerical value of the thermal inertia. It was suggested to change this parameter from 750 cm²-sec$^{\frac{1}{2}}$-°C/cal to 500, although this change has only slight effect on the temperature response curve.

In addition to the more realistic prediction of lunar crater temperatures, the consideration of thermal inertia in the heat balance equations suggests a qualitative explanation of localized temperature variations on the lunar surface. Saari and Shorthill[7] observed that some craters cooled less rapidly than their surrounding regions. This anomaly was quite pronounced at some craters, especially at Tycho. Although Tycho is shallow, its surroundings are rough, covered with smaller craters and other topographical features with significantly lower aspect ratios. To clarify this question, however, the transient solution of the crater heat balance equation may be required.

References

[1] Pettit, E. and Nicholson, B., "Lunar Radiation and Temperatures," *Astrophysical Journal*, Vol. 71, 1930, pp. 102–135.

[2] Jaeger, J. C., "The Surface Temperature of the Moon," *Australian Journal of Physics*, Vol. 6, 1953, pp. 10–21.

[3] Lucas, J. W. et al., "Lunar Temperatures and Thermal Characteristics," *Surveyor III Mission Report, Part II*, TR 32-1177, June 1967, Jet Propulsion Lab., Pasadena, Calif., pp. 155–188.

[4] Lucas, J. W. et al., "Lunar Surface Temperatures and Thermal Characteristics," *Surveyor V Mission Report, Part II*, TR 32-1246, Nov. 1967, Jet Propulsion Lab., Pasadena, Calif., pp. 89–113.

[5] Volterra, V., *Leçons sur les Equations Intégrales et les Equations Intégrodifférentielles*, Gautier-Villars, Paris, 1913.

[6] Courant, R. and Hilbert, D., *Methods of Mathematical Physics*, Interscience, New York, 1966, Chap. 3, pp. 140–142.

[7] Saari, J. M. and Shorthill, R. W., "Isotherms of Crater Regions on the Illuminated and Eclipsed Moon," *Icarus*, Vol. 2, 1963, pp. 115–136.

Effects of Base Pressure on Conical Thrust Nozzle Optimization

C. Marshall Byington Jr.*
Naval Air Systems Command, Washington, D. C.
AND
Joe D. Hoffman†
Purdue University, Lafayette, Ind.

Nomenclature

A_p, A_s = nozzle plane and spherical exit area, respectively
A_t, A_b = nozzle throat area and missile base area, respectively
C_{F_M} = missile thrust coefficient = $F/P_c A_t$
D = missile diameter
F = thrust
L = nozzle length
$\dot{m}$ = mass flow rate
M_s, M_∞ = nozzle-exit and freestream Mach numbers
p_b, P_c = base pressure and nozzle stagnation pressure
p_o, p_s = ambient and nozzle exit pressure, respectively
r, r_o, r_b = p_s/P_c, p_o/P_c, and p_b/P_c, respectively
R = spherical exit area radius of curvature
T_o, T_c = stagnation temperatures, freestream and nozzle
y_e, y_t = nozzle-exit and throat radii
α = nozzle cone half-angle
γ = specific heat ratio
Γ $\equiv \gamma^{1/2}[2/(\gamma + 1)]^{(\gamma+1)/2(\gamma-1)}$
λ = divergence loss factor $\equiv (1 + \cos\alpha)/2$
ξ $\equiv [2\gamma/(\gamma - 1)]^{1/2}$
ρ_t = throat radius of curvature
ϵ = nozzle area ratio = A_p/A_t
ϵ_g = geometrical area ratio = A_s/A_t
ϵ_r = gasdynamic expansion ratio based on pressure ratio r
η = base pressure correlation function

Superscript

$*$ = variable nondimensionalized by throat radius

Introduction

It was shown by Scofield and Hoffman[1] that the adapted or fully expanded conical nozzle does not yield maximum thrust, and the condition for maximum thrust was derived. However, in Ref. 1 and other studies which consider the design of a thrust nozzle alone, ambient pressure is generally assumed to surround the nozzle, and the effects that a flight ve-

Received December 22, 1969.
* Project Engineer. Student Member AIAA.
† Associate Professor of Mechanical Engineering. Member AIAA.

hicle may have on the nozzle environment and performance are not considered. In the event that the entire base of the vehicle is not filled by the submerged nozzle exit, some base area remains which can change the conditions for which the nozzle was designed, thereby affecting the performance obtained.

The pressure p_b acting on this base area depends on the free-stream Mach number and static pressure, the nozzle exit Mach number and static pressure, the specific heat ratios of the gases, the stagnation temperatures of the two streams, the nozzle cone angle, and the ratio of nozzle exit radius to missile radius. This paper presents a method for determining the cone angle of a fixed-length, conical nozzle which yields maximum thrust on the base of a propulsion vehicle with a specified diameter. Boundary layer and nonisentropic flow effects in the nozzle have been ignored. Only the vehicle base region is considered, since other vehicle drag is assumed to be fixed for fixed missile diameter and flight conditions. The flow around the vehicle is assumed to be at ambient conditions (i.e., M_∞ and p_o), an assumption which can easily be removed by an analysis of the flowfield around the vehicle.

Analysis

The usual assumptions[1] governing the one-dimensional, isentropic source flow of a thermally and calorically perfect gas are made. Only those vehicle parameters concerning p_b and vehicle thrust are considered. The thrust equation for the base of the propulsion vehicle is (see Fig. 1)

$$F = \lambda[\dot{m}V_s + A_s p_s] + A_b p_b \tag{1}$$

where V_s and p_s are evaluated on the spherical exit surface A_s, and p_b is evaluated on the annular surface A_b. As usual, the divergence loss factor λ is assumed to account for three-dimensional effects. The thrust coefficient for the vehicle base, defined as $C_{F_M} = F/P_c A_t$, is

$$C_{F_M} = \lambda\{\Gamma\xi[1 - r^{(\gamma-1)/\gamma}]^{1/2} + \epsilon_g r\} + [D^{*2} - \lambda\epsilon_g]r_b \tag{2}$$

For fixed values of γ, r_o, D^* L^*, ρ_t^*, and M_∞, the thrust coefficient is a function of the cone half-angle α and the nondimensionalized base pressure, $r_b = p_b/P_c$. The condition yielding maximum thrust is

$$dF/d\alpha = dC_{F_M}/d\alpha = 0 \tag{3}$$

Differentiating Eq. (1) and dividing by $d\alpha$ yields

$$p_s - p_b = \frac{A_b(dp_b/d\alpha) - \dot{m}V_s(\sin\alpha/2)}{(dA_b/d\alpha)} \tag{4}$$

In terms of nondimensionalized parameters, it can be shown that Eq. (4) is equivalent to

$$r - r_b = \frac{(\sin\alpha/2)\Gamma\xi[1 - r^{(\gamma-1)/\gamma}]^{1/2} - [D^{*2} - \lambda\epsilon_g]\,(dr_b/d\alpha)}{(d\epsilon_g/d\alpha) - \epsilon_g(\sin\alpha/2)} \tag{5}$$

To evaluate $dr_b/d\alpha$, an explicit relationship between p_b and α must be obtained. Data presented by Addy[2] relate

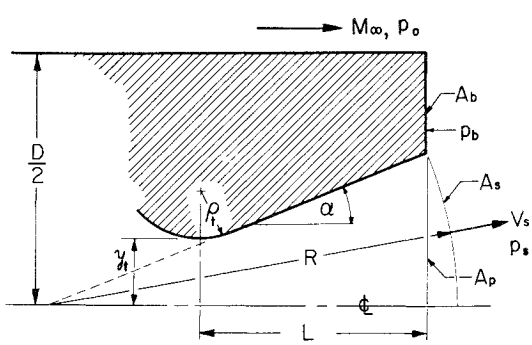

Fig. 1 Optimization model.

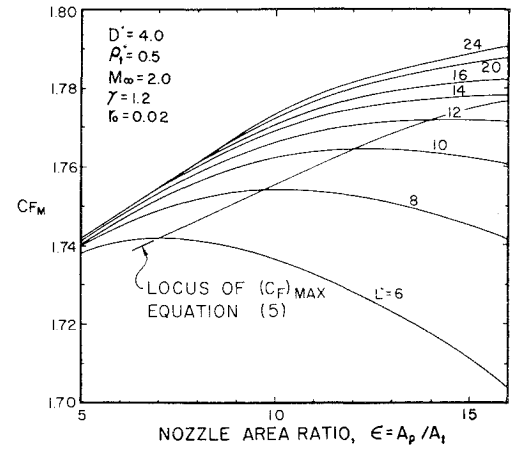

Fig. 2 Effect of geometry on performance.

p_b to p_o, p_s, M_∞, γ, M_s, α, T_o/T_c and $y_e/(D/2)$. We have correlated Addy's data by a curve fit of the form

$$(p_b/p_o) = f(p_s/p_o)\eta_{M_\infty}\eta_\gamma\eta_{M_s}\eta_\alpha\eta_{(T_o/T_c)}\eta_{y_e/(D/2)} \tag{6}$$

The six η functions are correction factors which are applied to the nominal case for which $f(p_s/p_o)$ was obtained; each factor accounts for variations in the parameter denoted by its subscript and was obtained by a curve fit of the form $\eta = \eta(p_s/p_o)$. Thus, Eq. (6) is a functional of the form $p_b = p_b(p_s)$. The nominal case was: $M_\infty = 2.0$, $\gamma = 1.2$, $M_s = 2.5$, $\alpha = 0°$, $(T_o/T_c) = 1.0$, and $(y_e/(D/2)) = 0.6$ The nozzle gasdynamic expansion ratio ϵ_r is related to the pressure ratio r by

$$\epsilon_r = \Gamma/\xi r^{1/\gamma}[1 - r^{(\gamma-1)/\gamma}]^{1/2} \tag{7}$$

The nozzle geometric area ratio ϵ_g is related to α, throat radius of curvature ρ_t^*, and length L^* by

$$\epsilon_g = A_s/A_t = 2R^{*2}(1 - \cos\alpha) \tag{8}$$

$$R^* = L^*\sec\alpha + \csc\alpha[1 + \rho_t^*(1 - \sec\alpha)] \tag{9}$$

We assume that $\epsilon_g = \epsilon_r$. Thus, for a fixed-length nozzle and a given ρ_t^*, Eqs. (7–9) yield a relationship of the form $p_s = p_s(\alpha)$, which, when combined with Eq. (6), yields $p_b = p_b(\alpha)$. The derivative $dr_b/d\alpha$ can then be evaluated by differentiating Eq. (6) with respect to p_s and multiplying by $dp_s/d\alpha$ obtained from Eqs. (7–9) with L^* and ρ_t^* fixed. Also, $d\epsilon_g/d\alpha$ can be found from Eqs. (6) and (7) to be

$$(d\epsilon_g/d\alpha) = 2R^*\{R^*\sin\alpha + 2(1 - \cos\alpha)[L^*\tan\alpha\sec\alpha - (1 + \rho_t^*)\cot\alpha\csc\alpha - \rho_t^*\csc^2\alpha(\tan^2\alpha - 1)]\} \tag{10}$$

Using the foregoing relationships and a suitable base pressure model, a value of nozzle pressure ratio satisfying Eq. (5) is the value which will yield maximum thrust and at the same time satisfy the imposed vehicle physical constraints. Equation (5) is solved for r by iterative techniques, using a FORTRAN computer program. Multiple solutions are found and some care must be exercised in choosing the proper one. In addition, certain combinations of the nondimensionalized parameters prove to be incompatible and do not permit a solution.

Examination of Eq. (5) shows that p_o does not appear in the optimization condition except for its influence on p_b. As would be expected, p_b does depend upon p_o and is considerably smaller than p_o. Therefore, for a nozzle of fixed L^*, the optimization should predict a smaller nozzle exit pressure and hence a larger area ratio than a nozzle designed for the ambient pressure. Predicted exit pressures were in all cases greater than p_b. Thus, flow separation due to over-expansion did not occur, since the back pressure seen by the nozzle flow is actually the base pressure. In some extreme cases, however,

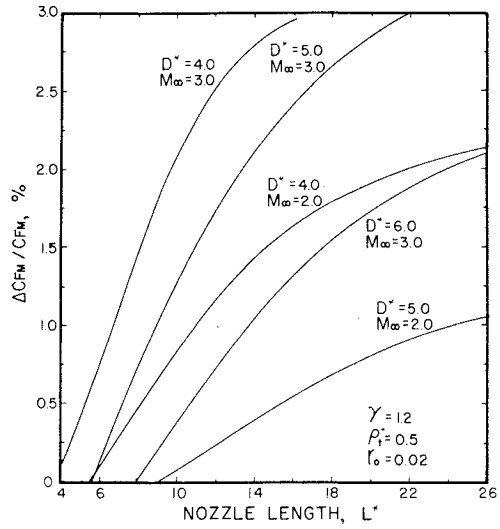

Fig. 3 Effect of vehicle size on performance.

it is possible that the flow could separate from the nozzle contour.

An analysis of the terms in Eq. (1) shows that expanding to lower pressures decreases the pressure thrust and base thrust. Base thrust decreases are a direct result of the coupling between r and r_b (p_s and p_b), since r_b decreases as r decreases. Divergence losses also increase, since larger cone angles are required to obtain larger area ratios with fixed nozzle length. However, the momentum thrust increases due to the increase in velocity brought about by the further expansion. It is obvious that the maximum thrust occurs at some point of trade-off between the above terms.

Figure 2 is a plot of Eq. (2) for a particular set of operating conditions, illustrating the thrust maximums discussed above. Also shown is the locus of $(C_F)_{MAX}$ determined from the design condition, Eq. (5). Long nozzles ($L^* > 12$) do not exhibit a thrust maximum except at the limiting case of no base area (i.e., $\epsilon = 16$). For a fixed L^*, the performance peak occurs at the trade-off point mentioned above, except for the long nozzles which completely fill the vehicle base. Similar trends were exhibited at different flight M_∞'s and vehicle area ratios (proportional to D^{*2}). Some care must be used to insure that the base-pressure model is valid for the base area under consideration.

For purposes of comparison, the optimum nozzles predicted by Scofield and Hoffman[1] for the specified operating conditions were placed in a vehicle of the same external diameter as considered in the present analysis. In cases involving relatively small-diameter vehicles operating at high r_o, the predicted optimum nozzle required an exit area larger than the proposed vehicle cross sectional area. This inconsistency cannot exist in the present analysis, since vehicle diameter is one of the imposed physical constraints in the optimization. It should be

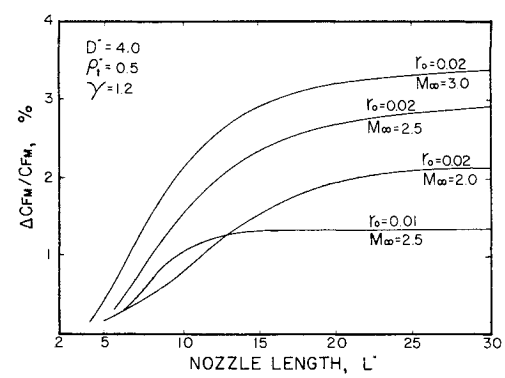

Fig. 4 Effect of flight conditions on performance.

pointed out here that the truncated perfect and Rao nozzles compared by Scofield and Hoffman[1] can also be compared to the results of the present analysis in a manner similar to the above. Figures 3 and 4 present the thrust improvement obtained by the present analysis over nozzles designed by the Scofield-Hoffman technique. These results are indicative of the performance increases obtainable using the proposed design technique. The magnitude of these improvements will depend upon the base pressure model employed. However, these results do exhibit trends which should be useful in designing conical thrust nozzles when an annular base region is present.

References

[1] Scofield, M. P. and Hoffman, J. D., "Optimization of Conical Thrust Nozzles," *Journal of Spacecraft and Rockets*, Vol. 4, No. 11, Nov. 1967, pp. 1547–1549.

[2] Addy, A. L., "Analysis of the Axisymmetric Base-Pressure and Base-Temperature Problem with Supersonic Interacting Freestream-Nozzle Flows Based on the Flow Model of Korst, et al.," RD-TR-69-12, July 1969, U.S. Army Missile Command, Redstone Arsenal, Ala.

Radiant Heat Transfer between Simply Arranged Surfaces with Direction Dependent Properties

J. S. Toor,* R. Viskanta,† and E. R. F. Winter‡
School of Mechanical Engineering, Purdue University, Lafayette, Ind.

RECENT investigations have shown that there is considerable discrepancy between the radiant heat-transfer predictions based on the diffuse, specular, and diffuse + specular analyses and experimental data[1,2] or more realistic direction-dependent property models.[1,3] The choice of the model for the radiation characteristics of surfaces is most critical for highly reflecting surfaces approaching the optically smooth condition.[1,2] The level of detail in the models which is needed in radiant heat transfer calculations has not been clearly established but appears to be most important when predicting local radiant energy quantities such as the flux, radiosity or irradiation.[3] This Note compares results for radiant heat-transfer calculations based on a directional emission and reflection model[1,3] with available experimental data.[2,4] A limited number of calculations based on the model were carried out and found to be promising.[1] The model appears to be a good compromise between realistic level of detail (where needed) and computational effort and is explored here in more detail. Results are reported for two configurations: 1) two parallel, infinitely long plates, and 2) two parallel, infinitely long plates separated on one edge by either a diffuse or a specular adiabatic plate (Fig. 1).

Model and Method of Solution

It is assumed that the geometric optics theory is valid for radiant heat transfer and that the surfaces are separated by a nonparticipating medium having an index of refraction of unity. The radiation surface characteristics and temperatures or heat transfer rates at the surfaces are assumed to be given.

Presented as Paper 69-624 at the AIAA 4th Thermophysics Conference, San Francisco, Calif., June 16–18, 1969; submitted December 12, 1969. Work supported by the NASA Manned Spacecraft Center under Contract NAS 9-8118.

* Research Assistant.
† Professor of Mechanical Engineering, Member AIAA.
‡ Professor of Mechanical Engineering.